Theoretical Investigation of the Reaction between Carbonyl Oxides and Ammonia

Solvejg Jørgensen

Copenhagen Center for Atmospheric Research, Department of Chemistry, University of Copenhagen, Universitetsparken 5, DK-2100 Copenhagen O, Denmark,

Allan Gross

Research Department, Danish Meteorological Institute, Lyngbyvej 100, DK-2100 Copenhagen O, Denmark

Received: December 9, 2008; Revised Manuscript Received: August 6, 2009

The gas-phase reaction between carbonyl oxides and ammonia is investigated by quantum mechanical calculations. The density functional method B3LYP with the basis set 6-311++G(2d,2p) was employed for the geometry and energy optimization of the stationary points along the reaction path. The energies have been refined by CCSD(T) with various basis sets and Gaussian-3 level of theory. The reaction mechanisms are studied for three different carbonyl oxides, H_2COO (methyl carbonyl oxide), CH_3HCOO (ethyl carbonyl oxide), and $(CH_3)_2COO$ (acetone carbonyl oxide). First, a prereactive complex is formed, where a hydrogen bond is formed between ammonia and the terminal oxygen atom in the COO moiety. Next, a structural rearrangement occurs, leading to the formation of a chemical bond between the nitrogen atom and the carbon in the COO moiety as well as a transfer of the hydrogen atom from nitrogen atom to the terminal oxygen atom in the COO moiety. The newly formed molecule is a hydroperoxide amine. All the studied reactions are exothermic. The estimated reaction rates range from 1.8×10^{-13} to 6.9×10^{-14} and to 5.1×10^{-18} cm^3 molecule^{-1} s^{-1} for H_2COO, CH_3HCOO, and $(CH_3)_2COO$, respectively. This shows that the investigated process are important in locations with intensive farming.

Introduction

Ammonia is a widespread atmospheric gas. The major source for atmospheric ammonia is volatilization from livestock waste; minor sources are fertilizers and a wide range of nonagricultural sources.[1] In intensive livestock areas, the NH_3 emission is on the order of 4−10 ton/km^2 per year, whereas in areas with little or no livestock area the emission is below 0.1 ton/km^2 per year.[2] In remote areas, the background level is less than 500 ppt,[3] whereas the concentration reaches a few parts per million in locations with intensive farming.[4] Due to the reduction of nitrogen oxides NO_X ($NO + NO_2$) to ammonia in the catalytic converters,[5] the atmospheric concentration of ammonia in urban areas has increased during the last years. Field studies in the urban area showed that the concentration of ammonia along the roadside is about five time the urban background level.[6] The sinks for emitted ammonia include oxidation by hydroxyl radicals and dry and wet deposition. Ammonia may react with inorganic and organic acids; these reactions may play a role in the formation of aerosol particle in the atmosphere.[7−9]

Aerosol particles affect the Earth's climate and the human health. The formation of new particles, so-called nucleation, is not fully understood. The binary nucleation between water and sulfuric acid cannot entirely explain the aerosol formation of atmospheric new particle formation.[10] Ternary water−sulfuric acid−ammonia nucleation[11,12] may also play an important role, and organic compounds can also influence the formation of aerosol particles. Aerosol particles were collected and their decomposition analyzed, they contained a substantial fraction of organic compounds.[13] Laboratory experiments have shown that the nucleation rate of sulfuric acid is enhanced in the presence of aromatic organic acids.[10] Just recently, it has been shown that ammonia reacting with organic acids influences the aerosol formation. Cocker and co-workers[8,9] have studied the formation of aerosol particles due to ozonolysis of styrene and α-pinene in the presence and absence of ammonia. In the experiment with styrene−ammonia, a decrease in the number of aerosol particles was observed as compared to the experiment without ammonia. The opposite trend was observed for α-pinene.

The emission of unsaturated hydrocarbons to the atmosphere is larger than 630 Tg C/year.[1] Their major degradation paths are reactions initiated by HO, NO_3, Cl, and ozone. Carbonyl oxides R_1R_2COO are formed in the reaction between ozone and unsaturated hydrocarbons. The ozonolysis follows the so-called Criegee mechanism[14] and is initiated with an addition of ozone to the double bond, forming a primary ozonide, which decomposes, leading to the formation of a carbonyl oxide (or Criegee intermediates) and a carbonyl compound. In the gas phase this reaction is highly exothermic, and therefore, the carbonyl oxide is vibrationally excited. It will either decompose unimolecularly or become collisionally stabilized.[15−17] Carbonyl oxides have not directly been detected and characterized during the ozonolysis, and most of the information on their molecular structure and the basic spectroscopic and thermochemical properties have been derived from quantum mechanical calculations. Just recently, Taatjes et al.[18] have been able to detect the carbonyl oxide H_2COO in the reaction between O_2 and dimethyl sulfoxide (DMSO). The collisionally stabilized carbonyl oxide reacts with the surrounding molecules in the atmosphere such as water,[19−23] hydroxyl radical,[24] nitrogen oxides,[25] sulfur dioxide,[17,25] carbon dioxide,[14] sulfuric acid,[26] aldehydes,[17,27−29] or carboxylic acid.[27,29,30] These reactions affect the tropospheric level of HO_x,[31] organic acids,[32,33] perioxides, and aerosol formation,[34,35] but their rate

* To whom correspondence should be addressed. E-mail: solvejg@kemi.ku.dk.

10.1021/jp905343u CCC: $40.75
Published on Web 08/27/2009

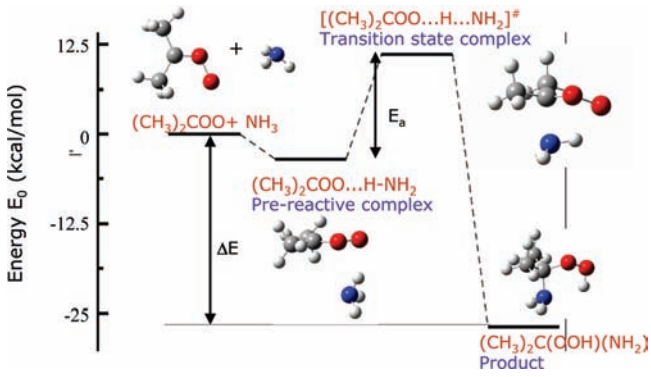

Figure 1. A schematic energy profile along the arbitrary reaction coordinate. The stationary points of the reaction between the carbonyl oxide and ammonia are shown. The carbonyl oxide involved in the displayed reaction is acetone carbonyl oxide $(CH_3)_2COO$. The energies corrected for zero-point vibrational energy are obtained at the G3 level of theory. The electronic energy is given in kcal/mol.

coefficients are poorly characterized and the product branching ratio is largely unknown. To date, only one direct kinetic study between methyl carbonyl oxide and acetaldehyde have been reported in the literature.[36] Bonn et al.[27,37] postulated that the organic/inorganic acids compete with water for reacting with carbonyl oxides; therefore, a large fraction of the aerosol particles in the atmosphere may be due to the reaction between carbonyl oxides and organic/inorganic acids.

The nucleation mechanism at microscopic level is still poorly understood. It is well-known that the nucleation rates are very sensitive to the thermodynamical properties of formation of complexes. The driving forces for the formation of complexes are hydrogen bonding. Theoretical calculations indicate that the formation of stable sulfuric acid−aromatic acid complex leads to a reduction of the nucleation barrier; this may explain the observed enhancement of binary sulfuric−water nucleation in the presence of a sub-part-per-billion level of organic acids.[10,38,39] Nadykto and Yu[40] investigated the thermodynamic stability of the molecular complexes of several atmospheric aerosol nucleating precursors (sulfuric acid, organic acid, water, and ammonia). Their results indicated that both organic acids and ammonia may efficiently enhance the binary sulfuric acid−water nucleation; furthermore, the organic acid interacts with ammonia. Zhao et al.[41] investigated the nature of the hydrogen bonds of complexes; the organic acids−sulfuric acid complexes tend to have stronger hydrogen bonds than in the organic acid−ammonia complexes. The binding energies of complexes of sulfuric acid are higher than for those with ammonia by usually several kilocalories/mole.

In the presented work, we investigate the bimolecular reaction mechanism between ammonia and carbonyl oxides using quantum mechanical calculations. In this investigation we have considered the reaction schematic shown in Figure 1. As far as we know, this is the first theoretical study of carbonyl oxide reacting with ammonia. The objectives of this paper are to investigate the reaction mechanism and to compute the reaction rate at 298.15 K for ammonia reacting with various carbonyl oxides. The analysis is based on ab initio quantum and statistical mechanical calculations.

Computational Details

All quantum mechanical calculations have been preformed with the Gaussian 03 program.[42] The geometries of the reactants, prereactive complexes, transition states, and products were examined using the Becke's three parameter hybrid density functional B3LYP method[43−45] with the basis set 6-311++G(2d,2p).[46] The threshold for the energy convergence in the self-consistent field (SCF) step was 1×10^{-16} au. The root-mean-square and maximum forces were converged to values less than 3×10^{-4} and 4.5×10^{-4} au, respectively. An ultrafine integration grid has been used in the calculations.

All the stationary points were characterized by their harmonic vibrational frequencies as minima or saddle points. Connections of the transition states between designated minima were confirmed in each case by the intrinsic reaction coordinate (IRC) calculation[47−49] with a step size of 0.05 $amu^{1/2}$ bohr. Zero point vibrational energies (ZPE) were determined from the harmonic vibrational frequencies; they are not corrected for the anharmonicity by introducing a scaling factor. The computed electronic energy is corrected for the zero point vibrational energy.

The optimized structures were also employed for single point energy optimization for refining the electronic energy by coupled-cluster theory with single and double excitations including perturbative corrections for the triple excitations (CCSD(T))[50] with several Gaussian-type basis sets.[46] In order to obtain the total energies, the CCSD(T) energies are corrected with the zero point vibrational energy estimated by B3LYP/6-311++G(2d,2p) calculations. Furthermore, Gaussian-3 level of theory (G3)[51] has been used to optimize and refine the energy.

Using single configurational methods like DFT or CCSD(T) may not be adequate for molecules with a biradical character like the carbonyl oxides. According to the CCSD(T)/aug-cc-pVTZ of Nguygen et al.,[52] the T1 diagnostic of H_2COO is 0.043; therefore, a single configurational method may be appropriate. Furthermore, they optimized the geometry of methyl carbonyl oxide using a complete active space self-consistent field (CASSCF) including 12 active electrons in 11 orbitals (six orbitals of a′ symmetry and five orbitals of a″ symmetry); this calculation indicates that both the contributions from the biradical and zwitterion character are small. Nguyen et al. concluded, therefore, that the single-reference CCSD(T) method sufficiently describes the electronic state of the carbonyl oxide. Furthermore, they also showed that the distance obtained by B3LYP is comparable with the CCSD(T) methods. We have carried out spin-unrestricted calculation (UB3LYP) for several of the mentioned structures. The energies and vibrational frequencies were identical for unrestricted and restricted B3LYP. Due to the above consideration, all the following calculation were carried out using spin-restricted B3LYP and CCSD(T).

We assume that the reaction between the carbonyl oxides and ammonia is a two-step mechanism:

$$\text{Step 1:}\quad R_1R_2COO + NH_3 \leftrightarrow R_1R_2COO\cdots H{-}NH_2 \tag{1}$$

$$\text{Step 2:}\quad R_1R_2COO\cdots H{-}NH_2 \rightarrow R_1R_2C(OOH)(NH_2) \tag{2}$$

The first step involves a fast pre-equilibrium between the reactants and the prereactive complex followed by an internal rearrangement leading to the formation of hydroperoxide alkyl amine. k_1 and k_{-1} are the forward and reverse rate constants for the first step (eq 1) and k_2 is the rate constant for the second step (eq 2). A steady-state analysis leads to the rate constant for the overall reaction

$$k_{tot} = \frac{k_1 k_2}{k_{-1} + k_2} \tag{3}$$

We assume that $k_2 \ll k_{-1}$, even though the barrier of the first step could be higher than that of the second step, and the above equation can be written as

$$k_{tot} = \frac{k_1}{k_{-1}} k_2 = K_{eq} k_2 \tag{4}$$

where K_{eq} stands for the equilibrium constant of the first step. It can be estimated by basic statistical thermodynamic principles[53] that

$$K_{eq} = \sigma \frac{Q_{RC}}{Q_{CI} Q_{NH_3}} \exp[-[E_{RC} - (E_{CI} - E_{NH_3})]/k_b T] \tag{5}$$

where Q_{CI} and Q_{NH_3} are the partition functions of the reactants and Q_{RC} is that for the prereactive complex. The total energies including the zero point energies are denoted E_{RC}, E_{CI}, and E_{NH_3} for the prereactive complex, carbonyl oxide, and ammonia, respectively. The constant σ is the symmetry factor counting the number of possible identical reaction paths. The rate constant for the second step can be evaluated using the standard transition state theory equation[53]

$$k_2 = \kappa \sigma \frac{k_b T}{h} \frac{Q_{TS}}{Q_{RC}} \exp[-(E_{TS} - E_{RC})/k_b T] \tag{6}$$

where Q_{TS} and E_{RC} are the partition function and energy of the transition state, whereas κ is the tunnelling factor. The tunnelling effect κ arises from quantum mechanical tunnelling through the potential energy barrier along the reaction coordinate. We have chosen the one-dimensional Wigner correction[54]

$$\kappa = 1 + \frac{1}{24}\left(\frac{h\nu}{k_b T}\right)^2 \tag{7}$$

which assumes that the tunnelling can only occur along the reaction coordinate. The frequency ν is the imaginary frequency of the transition state structure.

Results and Discussion

We have studied the reaction between ammonia and different carbonyl oxides: H_2COO (methyl carbonyl oxide), CH_3HCOO (ethyl carbonyl oxide), $(CH_3)_2COO$ (acetone carbonyl oxide). The syn configuration of $(CH_3)HCOO$ is more stable than the anti configuration, the energy difference being 2.64 and 3.38 kcal/mol at B3LYP/6-311++G(2d,2p) and G3 level of theory, respectively. The rational barrier between the two configurations is estimated to be 40 kcal/mol at B3LYP/6-311++G(2d,2p). The optimized structures of the studied carbonyl oxides are shown in Figure 2.

The bond lengths, angles and dihedrals of the reaction center between the COO moiety and ammonia are listed in Table S1 (Supporting Information). The total electronic energies and zero point vibrational energies of all the studied species are collected in Tables S2 and S3 (Supporting Information). The stabilization

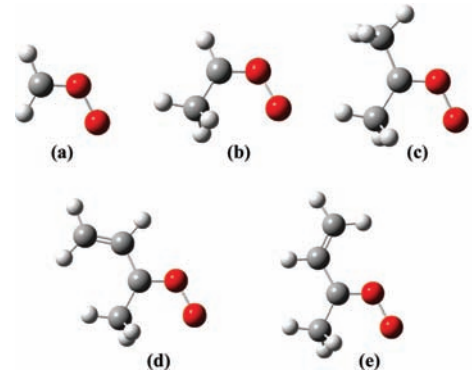

Figure 2. Structures of the carbonyl oxides studied in this work optimized at B3LYP/6-311++G(2d,2p) (white = hydrogen, gray = carbon, and red = oxygen atoms): (a) H_2COO, (b) *syn*-$(CH_3)HCOO$, (c) *anti*-$(CH_3)HCOO$, and (d) $(CH_3)_2COO$.

energy is defined as the energy difference between the prereactive complex and the reactants. The energy difference between the transition state structure and the prereactive complex is denoted as the activation barrier. The reaction energy is the energy difference between the product and the reactants. For all the studied reactions, the stabilization energy of the prereactive complex (E_{stab}), the activation barrier (E_a), and the reaction energy (ΔE_0) are presented in Table 1. All of these energies have been corrected for the zero point vibrational energy.

A. Reaction Mechanism. The reaction mechanism of the bimolecular reaction between ammonia and the carbonyl oxide can be described in two steps. First, a prereactive complex is formed; it is stabilized by a hydrogen bond between the terminal oxygen atom in the carbonyl oxide and one of the hydrogen atoms in the ammonia. Second, the hydrogen atom in the ammonia group is transferred to the terminal oxygen atom in the COO moiety; furthermore, a new chemical bond is formed between the nitrogen atom and the carbon atom. The newly formed molecule is a hydroperoxide alkylamine. Figure 1 shows a schematic energy profile along the arbitrary reaction coordinate.

The bimolecular reactions between carbonyl oxide and ammonia are exothermic for all the studied species (Table 1). The exothermicity decreases as the number of methyl group substitutions increases. The addition of methyl group leads to a stabilization of the COO group. The same trend was also observed for carbonyl oxide reacting with sulfuric acid or water.[22] Inclusion of the zero point vibrational energy leads to an energy of the reaction of −43.25 kcal/mol for the H_2COO at the CCSDT(T)/6-311+G(2d,2p)//B3LYP/6-311++G(2d,2p) level of theory. For H_2COO, the G3 level of theory and CCSD(T)/ 6-311+G(2d,2p)//B3LYP/6-311++G(2d,2p) are comparable.

As ammonia approaches the carbonyl oxide, a hydrogen bond between the terminal oxygen atom and one of the hydrogens in the ammonia is formed, leading to the formation of the prereactive complex. Structures of the prereactive complexes are shown in Figure 3. The length of the hydrogen bond ranges from 2.09 to 2.23 Å. The distance between the nitrogen atom and the α-carbon atom ranges from 2.9 to 3.8 Å; it tends to be shorter in the less substituted carbonyl oxides than in the more substituted and hindered ones. The chemical bonds of the carbonyl oxide fragment change very little compared to the original carbonyl oxide structure. In all the considered reactions, the hydrogen bond stabilizes the prereactive complex compared to the reactants. The B3LYP/6-311++G(2d,2p) tends to underestimate the stabilization energy of the prereactive complexes with a few kilocalories/mole (compared to the G3 level of

TABLE 1: Stabilization Energy of the Prereactive Complex (E_{stab}), the Activation Barrier (E_a), the Reaction Energy (ΔE_0) for the Reaction between Various Carbonyl Oxides and Ammonia[a]

reaction	method/basis set	E_{stab}	E_a	ΔE_0
$H_2COO + NH_3 \rightarrow$	B3LYP/6-311++G(2d,2p)	−3.73	2.99	−39.31
$H_2C(OOH)(NH_2)$	CCSD(T)/6-31+G(d)	−6.43	3.92	−43.13
	CCSD(T)/6-311+G(d,p)	−5.29	5.40	−44.69
	CCSD(T)/6-311+G(2d,2p)	−5.25	5.08	−43.25
	G3	−5.57	4.64	−43.28
syn-$(CH_3)HCOO + NH_3 \rightarrow$	B3LYP/6-311++G(2d,2p)	−3.32	9.38	−30.22
$(CH_3)HC(OOH)(NH_2)$	CCSD(T)/6-31+G(d)	−5.90	7.77	−36.82
	CCSD(T)/6-311+G(d,p)	−5.00	9.34	−39.21
	CCSD(T)/6-311+G(2d,2p)			
	G3	−4.88	9.05	−36.37
anti-$(CH_3)HCOO + NH_3 \rightarrow$	B3LYP/6-311++G(2d,2p)	−4.39	5.39	−33.95
$(CH_3)HC(OOH)(NH_2)$	CCSD(T)/6-31+G(d)	−7.83	5.20	−40.58
	CCSD(T)/6-311+G(d,p)	−6.77	6.27	−42.90
	CCSD(T)/6-311+G(2d,2p)			
	G3	−6.70	5.87	−40.72
$(CH_3)_2COO + NH_3 \rightarrow$	B3LYP/6-311++G(2d,2p)	−3.67	11.85	−25.09
$(CH_3)_2C(OOH)(NH_2)$	CCSD(T)/6-31+G(d)	−6.27	5.65	−34.75
	CCSD(T)/6-311+G(d,p)	−2.04	9.71	
	CCSD(T)/6-311+G(2d,2p)			
	G3	−5.97	10.36	−34.09

[a] The energies have been corrected for the zero point vibrational energy. All the electronic structure calculations are performed at different levels of theory. The CCSD(T) calculations are single point energy optimization using the B3LYP/6-311++G(2d,2p) geometries. The CCSD(T) calculations have been corrected by zero point vibrational energy from the B3LYP/6-311++G(2d,2p) calculations. The unit of the energy is kcal/mol.

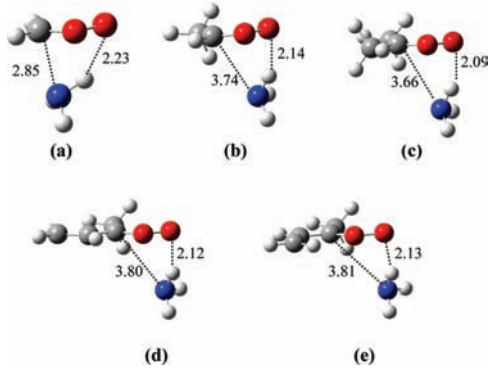

Figure 3. Structures of the prereactive complex studied in this work optimized at B3LYP/6-311++G(2d,2p) (green = nitrogen atoms): (a) $H_2COO\cdots H-NH_2$, (b) *syn*-$(CH_3)HCOO\cdots H-NH_2$, (c) *anti*-$(CH_3)_2COO\cdots H-NH_2$, and (d) $(CH_3)_2COO\cdots H-NH_2$. Distances are given in angstrøms.

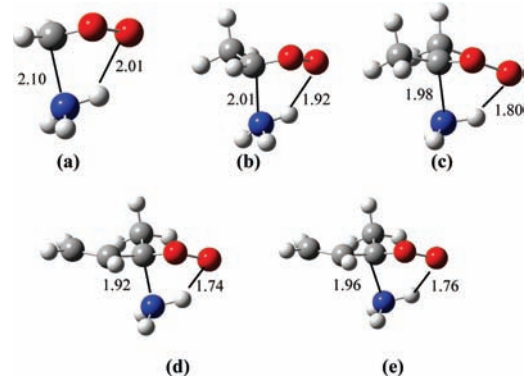

Figure 4. Structures of the transition-state complex studied in this work optimized at B3LYP/6-311++G(2d,2p): (a) $[H_2COO\cdots H\cdots NH_2]^{\#}$, (b) [*syn*-$(CH_3)HCOO\cdots H\cdots NH_2]^{\#}$, (c) [*anti*-$(CH_3)HCOO\cdots H\cdots NH_2]^{\#}$, and (d) $[(CH_3)_2COO\cdots H\cdots NH_2]^{\#}$. Distances are given in angstrøms.

theory). The single point energy optimization with CCSD(T) with the basis set (e.g., 6-311+G(d,p), 6-311+G(2d,2p)) using the B3LYP/6-311++G(2d,2p) geometries gives stabilization energies comparable with the one predicted by the G3 level of theory.

In the transition state structures, the nitrogen atom is approaching the carbon atom in the COO moiety, whereas the hydrogen bond is strengthening and the hydrogen atom is now approaching the terminal oxygen of −COO moiety (See Figure 4). In general, the hydrogen bond in the transition states structures is strengthening by approximately ∼0.3 Å compared to the prereactive complexes. The nitrogen atom gets closer to the carbon atom in the −COO moiety, and the distance between the nitrogen and the carbon atoms decreases with substitutions; it ranges from 1.97 to 2.10 Å in the reaction involving $(CH_3)_2COO$ and H_2COO, respectively. The reaction occurs later for the more substituted carbonyl oxides than for less substituted ones. The chemical bond between the two oxygen atoms elongates from 1.38 Å in the prereactive complexes to roughly 1.45 Å in the transition state structures. The chemical bond between carbon and oxygen is lengthening by ∼0.05 Å. In general, the activation barrier increases with the number of methyl group substitutions. We also observe that the activation barrier predicted by CCSD(T)/6-311+G(d,p) have the same magnitude as the G3 level of theory.

In the product structure, two new chemical bonds are formed, one between the hydrogen atom originally from the ammonia and the terminal oxygen atom of the COO moiety and the other one the between nitrogen atom. The length of the bond between oxygen and hydrogen is 0.97 Å, whereas the chemical bond between carbon and nitrogen ranges from 1.4 to 1.5 Å. The chemical bond between the two oxygen atoms is lengthening to 1.6 Å. The optimized structures of the products are shown in Figure 5.

B. Kinetics. All the partition functions used in the calculations for the rate constant of the reaction between carbonyl oxide and ammonia are given in Table S4 of the Supporting Information. The equilibrium constant for the first step (K_{eq}), the imaginary frequency of the transition state (ν), the one-dimensional Wigner tunneling correction (κ), rate constant of

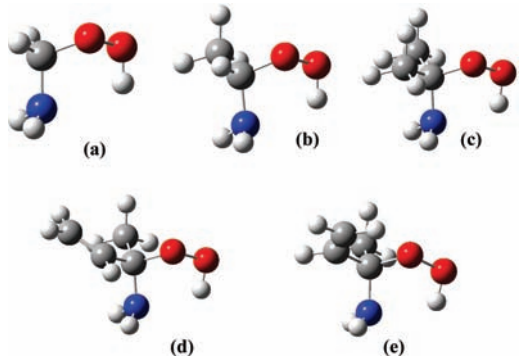

Figure 5. Structures of the products studied in this work optimized at B3LYP/6-311++G(2d,2p): (a) $H_2C(OOH)(NH_2)$, (b) *syn*-$(CH_3)HC(OOH)(NH_2)$, (b) *anti*-$(CH_3)HC(OOH)(NH_2)$, and (d) $(CH_3)_2C(OOH)(NH_2)$. Distances are given in angstrøms.

the second step (k_2), and the overall rate constant for the overall reaction (k_{tot}) are listed in Table 2.

A symmetry factor of 6 has been used in the calculation of the equilibrium constant, which counts the three equivalent hydrogen atoms on the ammonia and the two binding sites of ammonia; ammonia can attach to the carbon atom from below or above the molecular plane, leading to two different enantiomers of the prereactive complex. The two enantiomers have the same reaction path and corresponding energies. The equilibrium constants are on the order of $\sim 10^{-20}-10^{-23}$ cm^3 molecule^{-1} for all the studied reactions, depending on the methods and basis sets. The equilibrium constant is exponentially proportional to the stabilization energy of the prereactive complexes (E_{stab}), and it increases with increasing magnitude of the stabilization energy.

The imaginary frequencies describe the motion of a nitrogen atom toward the α-carbon atom as well as the motion of the hydrogen transfer from the nitrogen to the terminal oxygen atom in the −COO moiety. We observe that the imaginary frequency of the transition state structures increases with increasing number of methyl group substitutions; the same trend was observed for the magnitude of the activation barrier. Using the one-dimensional Wigner correction, the magnitude of quantum tunneling can be estimated; the quantum tunneling increased with increasing frequency of the reaction mode, i.e., the imaginary frequency. We can conclude that the tunneling may not play an important role, since the one-dimensional Wigner correction ranges from 1.05 to 1.13.

The rate constant for converting the prereactive complex into the products strongly depends on the activation barriers. The rate constant decreases with increasing activation barrier, and it is proportional to $\exp(-E_a/k_bT)$. It is important to emphasize at this point that for reactions that are barrierless (i.e., $E_{stab} + E_a < 0$), the approximation that the rate constant of the first step k_{-1} is much faster than that of the second step k_2 is not valid. For reactions with $E_{stab} + E_a > 0$, this approximation is valid. Although, we have estimated the overall rate constant for all the reactions under this approximation. At the G3 level of theory, the overall rate constant for the reaction between H_2COO and ammonia is 1.80×10^{-13} cm^3 molecule^{-1} s^{-1}, whereas the rate constants are 1.43×10^{-17}, 6.86×10^{-14}, and 5.1×10^{-18} cm^3 molecule^{-1} s^{-1} for *syn*-CH_3HCOO, *anti*-CH_3HCOO, and $(CH_3)_2COO$, respectively. The overall rate constants predicted by B3LYP/6-311++G(2d,2p) are underestimated with the expectation of H_2COO.

Conclusion

We have studied the reaction between three model species of carbonyl oxides and ammonia. The carbonyl oxides may react with ammonia, leading to the formation of hydroperoxide alkylamines. The energetic profiles along the reaction coordinate have been calculated by single point energy optimization by CCSD(T) with various basis sets using the B3LYP/6-311++G(2d,2p) optimized geometries. Further, we have also calculated the energetics with G3 level of theory. Comparing the stabilization energies, the activation barriers, and the reaction energies of the reaction $H_2COO + NH_3$ obtained by G3 and CCSD(T)/6-311+G(2d,2p)//B3LYP/6-311++G(2d,2p) level of theories, we concluded that the G3 level of theory is suitable

TABLE 2: The Equilibrium Constant (K_{eq}, cm^3 molecule^{-1}) of the First Step, the Imaginary Frequency (ν, cm^{-1}) of the Transition State Structure, the One-Dimensional Wigner Tunnelling Correction (κ, dimensionless), the Rate Constant (k_2, s^{-1}) of the Second Step, and the Total Reaction Rate Constant (k_{tot}, cm^3 molecule^{-1} s^{-1}) for the Overall Reaction[a]

reaction	method/basis set	K_{eq}	ν	κ	k_2	k_{tot}
$H_2COO + NH_3 \rightarrow$	B3LYP/6-311++G(2d,2p)	4.77×10^{-23}	238	1.05	2.71×10^{9}	2.18×10^{-13}
$H_2C(OOH)(NH_2)$	CCSD(T)/6-31+G(d)	4.56×10^{-21}			5.65×10^{8}	3.57×10^{-12}
	CCSD(T)/6-311+G(d,p)	6.64×10^{-22}			4.55×10^{7}	3.03×10^{-14}
	CCSD(T/6-311+G(2d,2p)	6.23×10^{-22}			7.97×10^{7}	4.96×10^{-14}
	G3	1.07×10^{-21}			1.68×10^{8}	1.80×10^{-13}
syn-$(CH_3)HCOO + NH_3 \rightarrow$	B3LYP/6-311++G(2d,2p)	2.38×10^{-23}	308	1.09	2.35×10^{4}	5.82×10^{-19}
$(CH_3)HC(OOH)(NH_2)$	CCSD(T)/6-31+G(d)	1.87×10^{-21}			3.55×10^{5}	6.83×10^{-16}
	CCSD(T)/6-311+G(d,p)	4.09×10^{-22}			2.62×10^{4}	1.07×10^{-17}
	CCSD(T/6-311+G(2d,2p)					
	G3	3.34×10^{-22}			4.28×10^{4}	1.43×10^{-17}
anti-$(CH_3)HCOO + NH_3 \rightarrow$	B3LYP/6-311++G(2d,2p)	8.79×10^{-23}	277	1.07	3.50×10^{7}	3.08×10^{-15}
$(CH_3)HC(OOH)(NH_2)$	CCSD(T)/6-31+G(d)	2.95×10^{-20}			4.77×10^{7}	1.41×10^{-12}
	CCSD(T)/6-311+G(d,p)	4.95×10^{-21}			7.96×10^{6}	3.94×10^{-14}
	CCSD(T/6-311+G(2d,2p)					
	G3	4.40×10^{-21}			1.56×10^{7}	6.86×10^{-14}
$(CH_3)_2COO + NH_3 \rightarrow$	B3LYP/6-311++G(2d,2p)	1.75×10^{-23}	328	1.10	4.83×10^{2}	8.47×10^{-21}
$(CH_3)_2C(OOH)(NH_2)$	CCSD(T)/6-31+G(d)	2.88×10^{-21}			1.26×10^{5}	3.63×10^{-16}
	CCSD(T)/6-311+G(d,p)	1.11×10^{-24}			1.78×10^{4}	1.99×10^{-20}
	CCSD(T/6-311+G(2d,2p)					
	G3	8.48×10^{-22}			6.01×10^{3}	5.10×10^{-18}

[a] All the electronic structure calculations are performed at different levels of theory. The CCSD(T) calculations are single point energy optimization using the B3LYP/6-311++G(2d,2p) geometries.

for investigation of the reaction between ammonia and larger carbonyl oxides. For all the considered reactions, we can conclude that the overall reaction is irreversible, due to the large thermal effect ($\Delta H \ll 0$).

We assume that the rate constant k_{-1} for transforming the prereactive complex into the reactants is much faster than the rate constant k_2 transforming the prereactive complex into products. Thereby we avoid estimating the forward and reverse rate constant for the first step, which involves a fast pre-equilibrium between the reactants and the prereactive complex. The formation of prereactive complex proceeds without a barrier, and the location of the transition state could be determined variationally by minimizing the reaction rate.[55]

Ryzhkov and Ariya[23] estimated the rate constant for the reaction between carbonyl oxides and a water molecule. For $H_2COO + H_2O$ the rate constant is estimated to be 8.2×10^{-18} cm^3 $molecule^{-1}$ s^{-1}. The ratio between the reaction rate for H_2COO reacting with ammonia and water is approximately 2×10^4. If the reaction between carbonyl oxide and ammonia should dominate compared to that of water, then the atmospheric concentration of ammonia should be 5×10^{-5} greater than the concentration of water. At 298 K and 5% relative humidity, the atmospheric concentration of water is roughly 1500 ppm. We can therefore conclude that the atmospheric concentration of ammonia must be on the order of parts per million if the reaction between carbonyl oxides and ammonia should play a significant role in the atmosphere. These high concentration levels can be reached in locations with intensive farming.[4]

The atmospheric degradation path of carbonyl oxide is decomposition and reaction with the surrounding molecules. The reaction between ammonia and carbonyl oxide may be a degradation path in areas with high concentration of ammonia and carbonyl oxide formed during ozonolysis of unsaturated hydrocarbons. This may not only occur in areas with intensive farming but also in cities with heavy traffic, since the concentration of ammonia is increasing due to the reduction of NO_x to NH_3 in catalytic converters on automobiles[5]

Acknowledgment. Danish Center for Scientific Computing is acknowledged for its support. S.J. is supported by Villum Kan Rasmussen Foundation (VKR), Danish Natural Science Research Council (FNU) (Project no. 272-05-0230), and Freia Fellowship from Faculty of Science, University of Copenhagen.

Supporting Information Available: The bond lengths, angles, and dihedrals of the reaction center between the COO moiety and ammonia are listed in Table S1. The total electronic energies and zero point vibrational energies are collected in Tables S2 and S3. All the partition functions used in the calculations for the rate constant are given in the Table S4. This material is available free of charge via the Internet at http://pubs.acs.org.

References and Notes

(1) Finlayson-Pitts, B. J.; Pitts, J. N. *Chemistry of the Upper and Lower Atmosphere*; Academic Press: San Diego, 2000.

(2) Vestreng, V.; Rigler, E.; Adams, M.; Kindbom, K.; Pacyna, J. M.; van der Gron, H. D.; Reis, S.; Travnikov, O. inventory review 2006, emission data reported to lrtap and nec directive, stage 1, 2 and 3 review and evaluation of inventories of hm and pops; Technical Report of the Norwegian Meteorological Institute; 2006; http://www.emep.int.

(3) Lewin, E. E.; Depena, R. G.; Shimshock, J. P. Atmospheric gas and particle measurements at a rural northeastern United States site. *Atmos. Environ.* **1986**, *20* (1), 59–70.

(4) Rumburg, B.; Mount, G. H.; Yonge, D.; Lamb, B.; Westberg, H.; Filipy, J.; Bays, J.; Kincaid, R.; Johnson, K. Atmospheric flux of ammonia from sprinkler application of dairy waste. *Atmos. Environ.* **2006**, *40* (37), 7246–7258.

(5) Matsumoto, R.; Umezawa, N.; Karaushi, M.; Yonemochi, S.; Sakamoto, K. Comparison of ammonium deposition flux at roadside and at an agricultural area for long-term monitoring: Emission of ammonia from vehicles. *Water Air Soil Pollut.* **2006**, *173* (1−4), 355–371.

(6) Perrino, C.; Catrambone, M.; Di Bucchianico, A. D. M.; Allegrini, I. Gaseous ammonia in the urban area of Rome, Italy and its relationship with traffic emissions. *Atmos. Environ.* **2002**, *36* (34), 5385–5394.

(7) Dinar, E.; Anttila, T.; Rudich, Y. CCN activity and hygroscopic growth of organic aerosols following reactive uptake of ammonia. *Environ. Sci. Technol.* **2008**, *42* (3), 793–799.

(8) Na, K.; Song, C.; Cocker, D. R. Formation of secondary organic aerosol from the reaction of styrene with ozone in the presence and absence of ammonia and water. *Atmos. Environ.* **2006**, *40* (10), 1889–1900.

(9) Na, K.; Song, C.; Switzer, C.; Cocker, D. R. Effect of ammonia on secondary organic aerosol formation from alpha-Pinene ozonolysis in dry and humid conditions. *Environ. Sci. Technol.* **2007**, *41* (17), 6096–6102.

(10) Zhang, R. Y.; Suh, I.; Zhao, J.; Zhang, D.; Fortner, E. C.; Tie, X. X.; Molina, L. T.; Molina, M. J. Atmospheric new particle formation enhanced by organic acids. *Science* **2004**, *304* (5676), 1487–1490.

(11) Ball, S. M.; Hanson, D. R.; Eisele, F. L.; McMurry, P. H. Laboratory studies of particle nucleation: Initial results for H_2SO_4, H_2O, and NH_3 vapors. *J. Geophys. Res.-Atmos.* **1999**, *104* (D19), 23709–23718.

(12) Weber, R. J.; McMurry, P. H.; Mauldin, R. L.; Tanner, D. J.; Eisele, F. L.; Clarke, A. D.; Kapustin, V. N. New particle formation in the remote troposphere: A comparison of observations at various sites. *Geophys. Res. Lett.* **1999**, *26* (3), 307–310.

(13) Kanakidou, M.; Seinfeld, J. H.; Pandis, S. N.; Barnes, I.; Dentener, F. J.; Facchini, M. C.; Van Dingenen, R.; Ervens, B.; Nenes, A.; Nielsen, C. J.; Swietlicki, E.; Putaud, J. P.; Balkanski, Y.; Fuzzi, S.; Horth, J.; Moortgat, G. K.; Winterhalter, R.; Myhre, C. E. L.; Tsigaridis, K.; Vignati, E.; Stephanou, E. G.; Wilson, J. Organic aerosol and global climate modelling: A review. *Atmos. Chem. Phys.* **2005**, *5*, 1053–1123.

(14) Criegee, R. Mechanism of ozonolysis. *Angew. Chem. Int. Ed. Engl.* **1975**, *14* (11), 745–752.

(15) Anglada, J. M.; Bofill, J. M.; Olivella, S.; Sole, A. Unimolecular isomerizations and oxygen atom loss in formaldehyde and acetaldehyde carbonyl oxides. A theoretical investigation. *J. Am. Chem. Soc.* **1996**, *118* (19), 4636–4647.

(16) Anglada, J. M.; Crehuet, R.; Bofill, J. M. The ozonolysis of ethylene: A theoretical study of the gas-phase reaction mechanism. *Chem. Eur. J.* **1999**, *5* (6), 1809–1822.

(17) Aplincourt, P.; Ruiz-Lopez, M. F. Theoretical investigation of reaction mechanisms for carboxylic acid formation in the atmosphere. *J. Am. Chem. Soc.* **2000**, *122* (37), 8990–8997.

(18) Taatjes, C. A.; Meloni, G.; Selby, T. M.; Trevitt, A. J.; Osborn, D. L.; Percival, C. J.; Shallcross, D. E. Direct observation of the gas-phase Criegee intermediate (CH_2OO). *J. Am. Chem. Soc.* **2008**, *130* (36), 11883–11885.

(19) Anglada, J. M.; Aplincourt, P.; Bofill, J. M.; Cremer, D. Atmospheric formation of OH radicals and H_2O_2 from alkene ozonolysis under humid conditions. *ChemPhysChem* **2002**, *3* (2), 215.

(20) Crehuet, R.; Anglada, J. M.; Bofill, J. M. Tropospheric formation of hydroxymethyl hydroperoxide, formic acid, H_2O_2, and OH from carbonyl oxide in the presence of water vapor: A theoretical study of the reaction mechanism. *Chem. Eur. J.* **2001**, *7* (10), 2227–2235.

(21) Hasson, A. S.; Chung, M. Y.; Kuwata, K. T.; Converse, A. D.; Krohn, D.; Paulson, S. E. Reaction of Criegee intermediates with water vapor—An additional source of OH radicals in alkene ozonolysis. *J. Phys. Chem. A* **2003**, *107* (32), 6176–6182.

(22) Kroll, J. H.; Sahay, S. R.; Anderson, J. G.; Demerjian, K. L.; Donahue, N. M. Mechanism of HO_x formation in the gas-phase ozone−alkene reaction. 2. Prompt versus thermal dissociation of carbonyl oxides to form OH. *J. Phys. Chem. A* **2001**, *105* (18), 4446–4457.

(23) Ryzhkov, A. B.; Ariya, P. A. A theoretical study of the reactions of parent and substituted Criegee intermediates with water and the water dimer. *Phys. Chem. Chem. Phys.* **2004**, *6* (21), 5042–5050.

(24) Mansergas, A.; Anglada, J. M. Reaction mechanism between carbonyl oxide and hydroxyl radical: A theoretical study. *J. Phys. Chem. A* **2006**, *110* (11), 4001–4011.

(25) Hatakeyama, S.; Kobayashi, H.; Akimoto, H. Gas-phase oxidation of SO_2 in the ozone olefin reactions. *J. Phys. Chem.* **1984**, *88* (20), 4736–4739.

(26) Kurten, T.; Bonn, B.; Vehkamaki, H.; Kulmala, M. Computational study of the reaction between biogenic stabilized Criegee intermediates and sulfuric acid. *J. Phys. Chem. A* **2007**, *111* (17), 3394–3401.

(27) Bonn, B.; Schuster, G.; Moortgat, G. K. Influence of water vapor on the process of new particle formation during monoterpene ozonolysis. *J. Phys. Chem. A* **2002**, *106* (12), 2869–2881.

(28) Neeb, P.; Horie, O.; Moortgat, G. K. The ethene−ozone reaction in the gas phase. *J. Phys. Chem. A* **1998**, *102* (34), 6778–6785.

(29) Tobias, H. J.; Ziemann, P. J. Kinetics of the gas-phase reactions of alcohols, aldehydes, carboxylic acids, and water with the C13 stabilized Criegee intermediate formed from ozonolysis of 1-tetradecene. *J. Phys. Chem. A* **2001**, *105* (25), 6129–6135.

(30) Neeb, P.; Sauer, F.; Horie, O.; Moortgat, G. K. Formation of hydroxymethyl hydroperoxide and formic acid in alkene ozonolysis in the presence of water vapour. *Atmos. Environ.* **1997**, *31* (10), 1417–1423.

(31) Heard, D. E.; Carpenter, L. J.; Creasey, D. J.; Hopkins, J. R.; Lee, J. D.; Lewis, A. C.; Pilling, M. J.; Seakins, P. W.; Carslaw, N.; Emmerson, K. M. High levels of the hydroxyl radical in the winter urban troposphere. *Geophys. Res. Lett.* **2004**, *31*, L18112.

(32) Becker, K. H.; Brockmann, K. J.; Bechara, J. Production of hydrogen-peroxide in forest air by reaction of ozone with terpenes. *Nature* **1990**, *346* (6281), 256–258.

(33) Gab, S.; Hellpointner, E.; Turner, W. V.; Korte, F. Hydroxymethyl hydroperoxide and bis(hydroxymethyl) peroxide from gas-phase ozonolysis of naturally-occurring alkenes. *Nature* **1985**, *316* (6028), 535–536.

(34) Johnson, D.; Marston, G. The gas-phase ozonolysis of unsaturated volatile organic compounds in the troposphere. *Chem. Soc. Rev.* **2008**, *37* (4), 699–716.

(35) Lee, S.; Kamens, R. M. Particle nucleation from the reaction of alpha-pinene and O-3. *Atmos. Environ.* **2005**, *39* (36), 6822–6832.

(36) Fenske, J. D.; Hasson, A. S.; Ho, A. W.; Paulson, S. E. Measurement of absolute unimolecular and bimolecular rate constants for CH_3CHOO generated by the *trans*-2-butene reaction with ozone in the gas phase. *J. Phys. Chem. A* **2000**, *104* (44), 9921–9932.

(37) Bonn, B.; Kulmala, M.; Riipinen, I.; Sihto, S. L.; Ruuskanen, T. M. How biogenic terpenes govern the correlation between sulfuric acid concentrations and new particle formation. *J. Geophys. Res. Atmos.* **2008**, *113*, D12209.

(38) McGraw, R.; Zhang, R. Y. Multivariate analysis of homogeneous nucleation rate measurements. Nucleation in the p-toluic acid/sulfuric acid/water system. 2. *J. Chem. Phys.* **2008**, *128*, 064508.

(39) Fan, J. W.; Zhang, R. Y.; Collins, D.; Li, G. H. Contribution of secondary condensable organics to new particle formation: A case study in Houston, Texas. *Geophys. Res. Lett.* **2006**, *33*, L15802.

(40) Nadykto, A. B.; Yu, F. Q. Strong hydrogen bonding between atmospheric nucleation precursors and common organics. *Chem. Phys. Lett.* **2007**, *435* (1−3), 14–18.

(41) Zhao, J.; Khalizov, A.; Zhang, R. Y.; McGraw, R. Hydrogen-bonding interaction in molecular complexes and clusters of aerosol nucleation precursors. 1. *J. Phys. Chem. A* **2009**, *113* (4), 680–689.

(42) Frisch, M. J.; Trucks, G. W.; Schlegel, H. B.; Scuseria, G. E.; Robb, M. A.; Cheeseman, J. R.; A., M.; J.; Vreven, T.; Kudin, K. N.; Burant, J. C.; Millam, J. M.; Iyengar, S. S.; Tomasi, J.; Barone, V.; B., M.; M, C.; G., S.; Rega, N.; Petersson, G. A.; Nakatsuji, H.; Hada, M.; Ehara, M.; Toyota, K.; Fukuda, R.; Hasegawa, J.; Ishida, K.; Nakajima, T.; Honda, Y.; Kitao, O.; Nakai, H.; Klene, M.; Li, X.; Knox, J. E.; Hratchian, H. P.; Cross, J. B.; Bakken, V.; Adamo, C.; Jaramillo, J.; Gomperts, R.; Stratmann, R. E.; Yazyev, O.; Austin, A. J.; Cammi, R.; Pomelli, C.; Ochterski, J. W.; Ayala, P. Y.; Morokuma, K.; Voth, G. A.; Salvador, P.; Dannenberg, J. J.; Zakrzewski, V. G.; Dapprich, S.; Daniels, A. D.; Strain, M. C.; Farkas, O.; Malick, D. K.; Rabuck, A. D.; Raghavachari, K.; Foresman, J. B.; Ortiz, J. V.; Cui, Q.; Baboul, A. G.; Clifford, S.; Cioslowski, J.; Stefanov, B. B.; Liu, G.; Liashenko, A.; Piskorz, P.; Komaromi, I.; Martin, R. L.; Fox, D. J.; Keith, T.; Al-Laham, M. A.; Peng, C. Y.; Nanayakkara, A.; Challacombe, M.; Gill, P. M. W.; Johnson, B.; Chen, W.; Wong, M. W.; Gonzalez, C.; Pople, J. A. Gaussian 03; 2003.

(43) Becke, A. D. Density-functional thermochemistry 0.3. The role of exact exchange. *J. Chem. Phys.* **1993**, *98* (7), 5648–5652.

(44) Lee, C. T.; Yang, W. T.; Parr, R. G. Development of the Colle−Salvetti correlation-energy formula into a functional of the electron-density. *Phys. Rev. B* **1988**, *37* (2), 785–789.

(45) Miehlich, B.; Savin, A.; Stoll, H.; Preuss, H. Results obtained with the correlation-energy density functionals of Becke and Lee, Yang and Parr. *Chem. Phys. Lett.* **1989**, *157* (3), 200–206.

(46) Hehre, W. J.; Radom, L.; Schleyer, R. R.; Pople, J. A. *Ab-Initio Molecular Orbital Theory*; Wiley: New York, 1986.

(47) Gonzalez, C.; Schlegel, H. B. An Improved algorithm for reaction-path following. *J. Chem. Phys.* **1989**, *90* (4), 2154–2161.

(48) Gonzalez, C.; Schlegel, H. B. Reaction-path following in mass-weighted internal coordinates. *J. Phys. Chem.* **1990**, *94* (14), 5523–5527.

(49) Ishida, K.; Morokuma, K.; Komornicki, A. Intrinsic reaction coordinate−An abinitio calculation for $HNC^-]HCN$ and $H^-+CH_4{}^-]CH_4+H^-$. *J. Chem. Phys.* **1977**, *66* (5), 2153–2156.

(50) Pople, J. A.; Headgordon, M.; Raghavachari, K. Quadratic configuration−interaction−A general technique for determining electron correlation energies. *J. Chem. Phys.* **1987**, *87* (10), 5968–5975.

(51) Curtiss, L. A.; Raghavachari, K.; Redfern, P. C.; Rassolov, V.; Pople, J. A. Gaussian-3 (G3) theory for molecules containing first- and second-row atoms. *J. Chem. Phys.* **1998**, *109* (18), 7764–7776.

(52) Nguyen, M. T.; Nguyen, T. L.; Ngan, V. T.; Nguyen, H. M. T. Heats of formation of the Criegee formaldehyde oxide and dioxirane. *Chem. Phys. Lett.* **2007**, *448* (4−6), 183–188.

(53) McQuarrie, D. A. *Statistical Mechanics*; Harper Collins Publisher: New York, 1976.

(54) Wigner, E. Concerning the excess of potential barriers in chemical reactions. *Z. Phys. Chem., Abt. B* **1932**, *19* (2/3), 203–216.

(55) Lei, W. F.; Zhang, R. Y.; McGivern, W. S.; Derecskei-Kovacs, A.; North, S. W. Theoretical study of isomeric branching in the isoprene−OH reaction: Implications to final product yields in isoprene oxidation. *Chem. Phys. Lett.* **2000**, *326* (1−2), 109–114.

JP905343U